CHINESE OPTICS LETTERS

Vol. 21, No. 5 | May 2023

Enhanced near-infrared light-induced photoresponse via transition of monocrystalline phase and surface reconstruction

Hong Jia (贾 红)[1*,†], Hongming Jiang (蒋洪明)[1,2,†], Yuping Zhang (张瑜萍)[1], Shuxu Hua (华淑旭)[1], Qing Liu (刘 青)[1], Yuquan Yuan (袁玉全)[2], Yanfei Hu (胡燕飞)[3**], Feng Peng (彭 枫)[1***], and Xiaofeng Liu (刘小峰)[4****]

[1] College of Physics and Electronic Information & Key Laboratory of Electromagnetic Transformation and Detection of Henan Province, Luoyang Normal University, Luoyang 471934, China

[2] School of Physics and Electronic Engineering, Sichuan University of Science & Engineering, Zigong 643000, China

[3] Department of Applied Physics, Chengdu University of Technology, Chengdu 610059, China

[4] School of Materials Science and Engineering, Zhejiang University, Hangzhou 310027, China

*Corresponding author: jiahong517@aliyun.com

**Corresponding author: yanfeihususe@suse.edu.cn

***Corresponding author: fpeng@lynu.edu.cn

****Corresponding author: xfliu@zju.edu.cn

Received January 4, 2023 | Accepted March 10, 2023 | Posted Online April 13, 2023

Rare-earth-doped upconversion (UC) materials are ideal candidates for solar photovoltaic conversion and NIR response devices due to their unique spectral conversion properties. However, their low efficiency remains a tremendous challenge for practical applications. Here, we constructed an efficient NIR light-responsive device by coating a Si-photoresistor with a transparent gel consisting of UC powders and an organic polymer matrix. We show that reasonable introduction of alkali metal ions (Na^+, K^+, and Cs^+) into the lattice of UC crystals results in the improvement of photoelectricity conversion efficiency, due to the high crystallinity and surface reconstruction caused by alkali metal ion doping.

Keywords: rare-earth-doped upconversion materials; solar photoelectric conversion; NIR response devices; doping with alkali metals.

DOI: 10.3788/COL202321.051603

1. Introduction

Upconversion (UC) luminescent materials have been extensively used in display imaging, sensing detection, photothermal therapy, and photovoltaics because of their peculiar optical process[1–7]. Metal ions with the d, f orbitals can fulfill the requirement for the UC by virtue of their long-lived excited states and ladder-level configurations[8]. In addition, a large number of transition metals and actinide-doped materials have been reported to display UC properties[9]. Among them, lanthanide-doped UC solid materials show superior upconversion luminescence (UCL) characteristics, and fluoride and sulfide UC materials with low phonon energies are the ideal host matrix[10,11]. However, the matrix is being replaced by oxide materials due to its poor stability and high toxicity. In oxide UC materials, the inherent structural defects, low absorption cross section, and dipole transitions of the rare-earth ions usually result in a low UC efficiency. Up to the present, several strategies have been developed to optimize the materials design and to improve the efficiency of oxide UC materials.

In order to reduce the quenching effect of surface defects or surface-related ligands, a core-shell structure is one of the solutions. For example, Vetrone *et al.* reported the use of "active" doped shells to increase surface passivation to reduce nonradiative transition rates and to enhance UCL[12]. Liu *et al.* also achieved a significant enhancement of the UCL by adding a microlens array to the top of the UC nanomaterial to modulate the temporal distribution of transmitted excitation photons[13,14]. However, the UC process is still relatively inefficient due to the inherently low absorption coefficients of rare-earth (RE) ions. This problem can be mitigated by using dye sensitization for RE ions, and the combination of dye sensitization with a core-shell structure could lead to higher efficiency. For instance, Shao and coworkers introduced the organic dye indocyanine green (ICG) onto the surface of core-shell structured $NaYF_4$-based UC particles[15], which demonstrated a large

increment in UC emission intensity several times and enabled a wider excitation band. However, organic dyes are not suitable for long-term solar illumination due to their poor molecular stability and susceptibility to competitive energy loss during heterogeneous energy transfer. In atomic spectroscopy, electric dipole transition is one of the most important transitions in the process of the atom/nucleus emission or absorption of photons[16]. The lack of an electric dipole moment will result in prohibition of transition. Photonic crystal (Phc) structure engineering by incorporation of upconverting nanoparticles (UCNPs) into a photonic lattice could boost the UC intensity due to the enhanced local electric field under NIR excitation[17]. A similar strategy for electric field enhancement based on plasmonic structures has also been found to be highly effective in enhancing the UC emission[18–23], but the use of precious metals and the high fabrication cost make it difficult for larger-scale applications.

In the above UCL enhancement mechanisms, local field modulation and surface optimization are always the most efficient strategies. Due to the influence of many restrictive conditions on the photovoltaic conversion, we here chose surface engineering strategy by using non-RE ions doping to adjust the atomic structure of the UCNPs' surface and to control structure transition from amorphous to ordered crystal to increase the absorption efficiency and enhance the luminescence efficiency. Due to the low phonon energy, excellent thermal stability, high physical durability, and the close cation ionic radius, Gd_2O_3 is considered as a good host material for rare-earth ions[24,25]. Er^{3+} ions with ladder energy levels and long excited state life are considered the most suitable UC activator[26–28]. In addition, we consider that the local fields and surface microstructure may be changed by doping with alkali metal ions due to the differences in ionic radii and the electronegativity. Although most previous work employed Li^+ ions as the co-dopant[29,30], we show that $Gd_2O_3:Er^{3+}$, X (X = Na^+, K^+, Cs^+) exhibits large enhancements in UC emission compared with the phosphor without the introduction of alkali metal elements. In addition, we propose a low-cost strategy that rationally integrates the UC particles with Si-based photoresistors (Si-BPRs) for NIR responsive devices. With the conversion of the NIR (> 750 nm) photons into visible light (400 to 700 nm) by UC materials, the developed device demonstrates strong electrical responses to NIR light, suggesting its potential use in NIR sensing and detection.

2. Experiment Section

Synthesis of Gd_2O_3:Er^{3+}, M^+ (M = Cs, K and Na) phosphors. MNO_3 (M = Cs, K and Na, 99%), $RE(NO_3)_3 \cdot 6H_2O$ (RE = Gd, Er, 99.99%), $C_2H_6O_2$ (99.5%), $C_6H_8O_7$ (99%), and H_3BO_3 (99%) were used as raw materials. $Gd_2O_3:xEr^{3+}$ (x = 1%, 3%, 5%, 7%, 10%, 12%, molar fractions), yM^+ (y = 1%, 3%, 5%, 7%, 10%, 12%, molar fractions) phosphors were synthesized by the low-temperature combustion method. All samples were synthesized with the same procedure detailed as follows. (1) Appropriate amounts of MNO_3, $RE(NO_3)_3 \cdot 6H_2O$, and H_3BO_3 were dissolved in water to form a solution of 0.1 mol/L. (2) 17.5 mL of $Gd(NO_3)_3 \cdot 6H_2O$, 0.525 mL of $Er(NO_3)_3 \cdot 6H_2O$, 1 mL of $C_2H_6O_2$, 2.2447 g of $C_6H_8O_7$, and an appropriate amount of MNO_3 were added into a 50 mL beaker, and the solution mixture was stirred for 0.5 h. (3) 17.5 mL of H_3BO_3 was added into the beaker, and stirring was kept for 3 h until the sample was fully dissolved. (4) The samples were transferred to a crucible and placed in an oven at 100°C for 18 h for full reaction. (5) After annealing at 800°C for 3 h, the samples were collected after cooling to ambient temperature.

Fabrication of the spectral converter based on the PMMA composite film. (1) 1 g of polymethylmethacrylate (PMMA) powder and 10 mL of dimethyl formamide (DFM) were added to a beaker and stirred at 50°C for 1 h to form a viscous gel. (2) 0.03 g of $Gd_2O_3:Er^{3+}$, M^+ phosphor was added to the above gel and fully dispersed. (3) The transparent gel was coated on the surface of hydrogenated amorphous silicon and placed in a drying oven at 70°C for 12 h. Finally, a hybrid film made of the UC composite film and the semiconductor (a-Si) was fabricated.

Characterization of structure and performance. The surface morphology of phosphors was measured by a scanning electron microscope (SEM) (Regulus 8100). Transmission electron microscopy (TEM) images, mapping element distributions, and selective area electron diffraction (SAED) patterns were obtained with an electron microscope (FEI Tecnai G2 F20). The phase characteristics of phosphor particles were studied by an X-ray diffractometer (XRD) (Bruker D8 Advance). The absorption spectra of the samples were recorded with a UV-VIS spectrophotometer (U3600P) by using a barium sulfate substrate as the background reference. The spectral characteristics were recorded under excitation by a 980 nm laser diode with two Zolix spectrometers (Omni-λ3007, Omni-λ180D). The voltage-time characteristics were analyzed by using a homemade device consisting of an excitation source (980 nm), a mixed domain oscilloscope, and related circuits.

3. Results and Discussion

3.1. Structural and morphological characteristics

In order to observe the morphology of changes of its morphology and structure after the introduction of alkali metals, the $Gd_2O_3:3\%\ Er^{3+}$ and $Gd_2O_3:3\%\ Er^{3+}$, M^+ (M = Na, K, Cs) phosphors were recorded by an SEM. As shown in Fig. 1(a), the $Gd_2O_3:3\%\ Er^{3+}$ phosphor particles exhibit a tabular structure with a radius of 80–300 nm. After the introduction of Na^+ and K^+ ions, the tabular structure was significantly changed. Figures 1(b) and 1(c) show that the size of nanoparticles doped with Na^+ and K^+ ions is 60–100 nm and 60–250 nm, respectively. In addition, the introduction of a large number of Cs^+ with large ionic radii leads to the formation of bar (30–130 nm) and columnar (230–450 nm) morphologies. The possible mechanism of morphology evolution after introducing Cs^+ ions into $Gd_2O_3:3\%\ Er^{3+}$ phosphor is proposed as follows. The

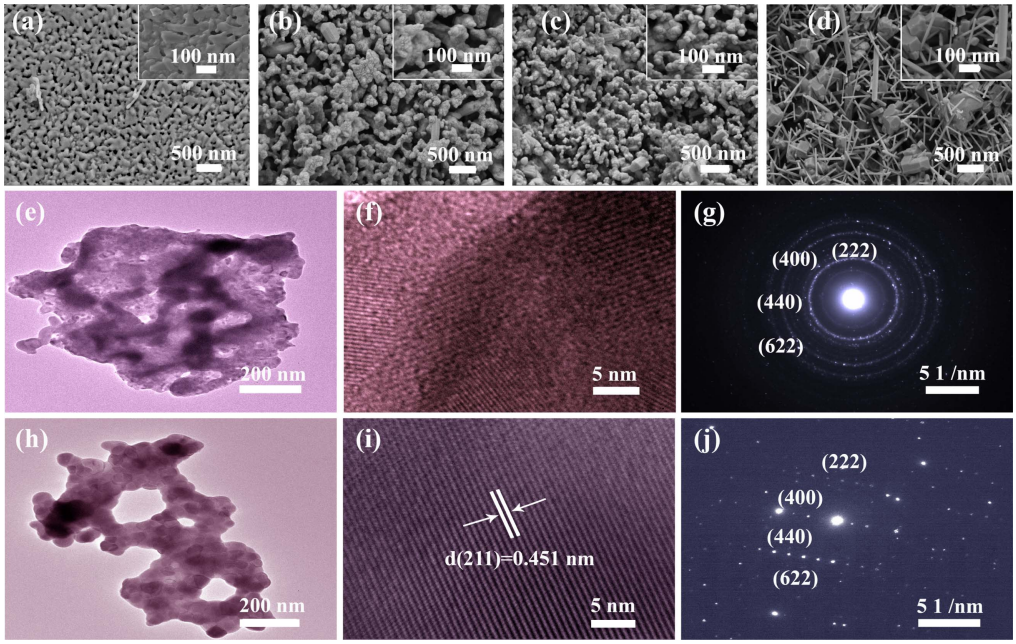

Fig. 1. SEM images of the synthesized samples: (a) Gd_2O_3: 3% Er^{3+}; (b) Gd_2O_3: 3% Er^{3+}, 10% Na^+; (c) Gd_2O_3: 3% Er^{3+}, 7% K^+; (d) Gd_2O_3: 3% Er^{3+}, 3% Cs^+. (e), (h) TEM images; (f), (i) HRTEM images; (g), (j) SAED patterns of Gd_2O_3: 3% Er^{3+} and Gd_2O_3: 3% Er^{3+}, 10% Na^+ phosphors.

Cs^+ ions likely enter into interstitial sites due to their different valence states with Gd^{3+} ions when Cs^+ is introduced into the Gd_2O_3 matrix. Similar to the vast number of Li^+ ions doping, this will inevitably cause some lattice distortion[31–33]. However, doping a large number of Cs^+ ions with large ionic radii may cause a greater degree of lattice distortion and even restrict the periodic arrangement of some crystal planes. The high chemical potential energy at high temperatures results in the rapid aggregation of primary particles. While the continuous self-assembly of easily grown crystal faces in the process of mutual reactions results in long columnar and strip-like forms with the same lattice orientation [Fig. 1(d), and Fig. S3(d) in the Supplementary Material][34], the analysis of $Gd_2O_3:3\%\ Er^{3+}$/ $Gd_2O_3:3\%\ Er^{3+}$, 10% Na^+ phosphors by TEM, high-resolution transmission electron microscopy (HRTEM), and SAED is helpful for further observation of their morphological characteristics. As shown in Figs. 1(e) and 1(h) transmission microscopic images, a $Gd_2O_3:3\%\ Er^{3+}$ phosphor is formed by the polymerization of particles with a diameter of about 20–40 nm. The introduction of Na^+ ions greatly reduced the phosphor agglomeration phenomenon and increased the size of nanoparticles to about 60 nm, which is similar to the results obtained in Table S1 (Supplementary Material). On the other hand, the transmission amplification results in Fig. 1(e) indicate that the 80–300 nm tabular structure in Fig. 1(a) may be composed of smaller particles with a diameter of about 20–40 nm, while the introduction of alkali metals is conducive to reducing the agglomeration phenomenon. Meantime, HRTEM showed different lattice fringes [Figs. 1(f) and 1(i)]. Compared with $Gd_2O_3:3\%\ Er^{3+}$, the introduction of Na^+ ions contributes to the formation of the monocrystalline phase, and the interplanar spacing is about 4.51 Å (211 planes). This is undoubtedly beneficial for many aspects, such as eliminating high dislocation defects or high concentrations of impurities. In addition, the SAED patterns given in Figs. 1(g) and 1(j) can be indexed to the (222), (400), (440), and (622) planes of cubic Gd_2O_3. Therefore, for $Gd_2O_3:3\%\ Er^{3+}$ and $Gd_2O_3:3\%\ Er^{3+}$, 10% Na^+ phosphors, although the doping of Na^+ ions caused a large change in particle morphology, it only leads to a small change in the phase. In addition, the morphologic features of K^+- and Cs^+-doped $Gd_2O_3:3\%\ Er^{3+}$ are shown in Fig. S3 (see Supplementary Material).

3.2. Optical performance

The absorption spectra and the emission spectra of the samples prepared under different conditions were studied. Figure 2(a) presents the absorption spectra for $Gd_2O_3:3\%\ Er^{3+}$ and $Gd_2O_3:3\%\ Er^{3+}$, $y\mathrm{M}^+$ (M = Na, K, Cs; y = 10%, 7%, 3%). All samples showed the expected absorption peaks at 808 and 980 nm. For the absorption peak at 980 nm, it was found that the absorption peak was enhanced when Na^+ ions were added, but the introduction of K^+ and Cs^+ ions had no observable effect. In addition, the UC photoluminescence (PL) spectra of the samples are greatly affected by the doping of different concentrations of active ions. Therefore, the PL emission spectra of the prepared samples were studied in more detail. Figure 2(b) shows the emission spectra of $Gd_2O_3:x\mathrm{Er}^{3+}$ (x = 1%, 3%, 5%, 7%, 10%, 12%) phosphors excited by a 980 nm laser. All the PL spectra showed the same spectral shape and reached the maximum peak at the green region (539–570 nm). When the concentration exceeds 3%, the PL intensity decreases notably as a result of concentration quenching. It is also possible that the

solubility limit of Er^{3+} in the Gd_2O_3 lattice is smaller considering the mismatch in ionic size. In order to explore the effect of alkali metal ions (Na^+, K^+, Cs^+) on the luminescence of phosphors, the PL emission spectra of corresponding phosphors were studied. For Gd_2O_3 : 3% Er^{3+}, 10% Na^+ phosphors in Fig. 2(c), the peak position does not move with the addition of Na^+ ions. This indicates that the introduction of Na^+ ions can significantly increase the intensity of the emission peak in the Gd_2O_3 : Er^{3+} phosphors, but the local structure of Er^{3+} remains unchanged. The luminescence is strongest when the concentration of Na^+ ions reaches 10%. Similarly, the optimal concentrations of K^+ and Cs^+ ions were 7% and 3%, respectively [Fig. 2(d)], and the emission intensities were ordered as 10% Na^+ > 3% Cs^+ > 7% K^+. The spectral result in Fig. 2(d) shows that the strongest peak is located at 563 nm. In addition, the left image of Fig. 2(d) shows the visible green luminescence of the samples at 980 nm excitation. The results shown in the green luminescence diagram are fully synchronized with the curve in Fig. 2(d), which further proves that the addition of alkali metals (Na^+/K^+/Cs^+) can significantly improve the luminescence intensity.

Here, we also recorded the luminescence intensity of Gd_2O_3 : 3% Er^{3+}, M (M = 10% Na^+, 7% K^+, and 3% Cs^+) samples after 60 days at room temperature. As shown in Fig. S3(a) (see Supplementary Material), Gd_2O_3 : 3% Er^{3+}, 3% Cs^+ phosphors show a large intensity attenuation with the increase of storage time. There is no doubt that this is closely related to prolonged exposure to air. The possible reason is that the Cs^+ ions could interact with water molecules in air, which results in the weakening of the luminescence intensity with time. Fortunately, the emission intensity of Gd_2O_3 : 3% Er^{3+}, 3% Cs^+ phosphors before storage is comparable to that of Na^+-doped phosphors [Fig. 2(a)]. There are two reasons for this. (1) The Cs^+ ion has the strongest metal properties, the position of lowest unoccupied molecular orbital (LUMO) level increases and the forbidden bandwidth becomes narrower when it enters into the Gd_2O_3 matrix, leading to the enhancement of the transition probability from highest occupied molecular orbital (HOMO) level to the conduction band. (2) The introduction of Cs^+ ions optimized the surface properties of the phosphor. Compared with the polycrystalline phase for the K^+ ion-doped samples [Figs. S3(b) and S3(c) in the Supplementary Material], the Gd_2O_3 : 3% Er^{3+}, 3% Cs^+ phosphor forms a single crystal phase that is beneficial to generate efficient PL [Figs. S3(e) and S3(f) in the Supplementary Material] because compared with the polycrystalline phase, the monocrystalline phase is more favorable to the light refraction and scattering process. However, the vacuum environment becomes a necessary condition for the practical application of Gd_2O_3 : 3% Er^{3+}, 3% Cs^+ phosphors considering the high sensitivity to air. Figure 2(e) shows PL emission spectra as a function of annealing temperature. Obviously, with the increase in annealing temperature, the luminescence intensity increases continuously and reaches its maximum at 1100°C. The luminescence images in the inset of Fig. 2(e) again substantiate the obvious enhancement of luminescence intensity at 1100°C. To visualize the emission of the phosphor, the Commission International de l'Eclairage (CIE)

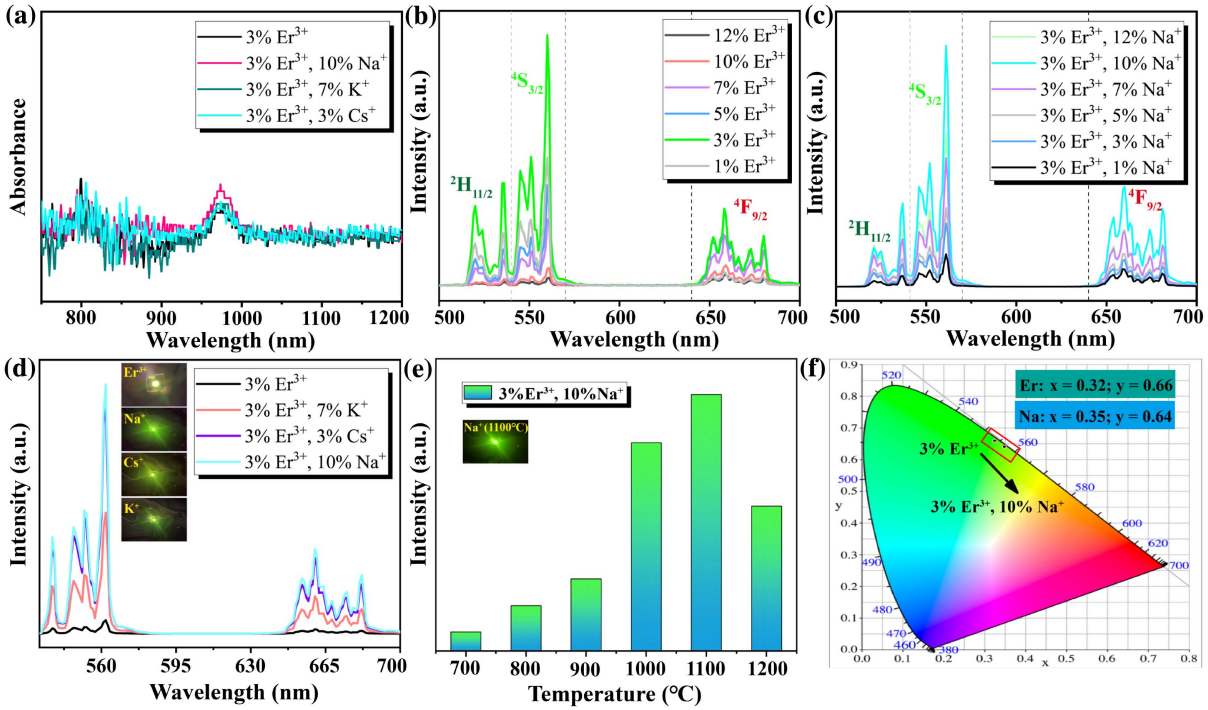

Fig. 2. (a) Absorption spectra of Gd_2O_3: 3% Er^{3+} and Gd_2O_3: 3% Er^{3+}, yM^+ (M = Na, K, Cs; y = 10%, 7%, 3%). UC PL emission spectra for (b) Gd_2O_3: xEr^{3+} (x = 1%, 3%, 5%, 7%, 10%, 12%); (c) Gd_2O_3: 3% Er^{3+}, yNa^+ (y = 1%, 3%, 5%, 7%, 10%, 12%); and (d) Gd_2O_3: 3% Er^{3+}, zM^+ (M = Na, K, Cs; z = 10%, 7%, 3%). (e) Luminescence intensity of the Gd_2O_3: 3% Er^{3+}, 10% Na^+ phosphors at different annealing temperatures; (f) CIE chromaticity diagram of the Gd_2O_3: 3% Er^{3+} and the Gd_2O_3: 3% Er^{3+}, 10% Na^+ phosphors.

1931 chromaticity coordinates pattern of the $Gd_2O_3:3\%\ Er^{3+}$ and $Gd_2O_3:3\%\ Er^{3+}, 10\%\ Na^+$ samples are calculated. As shown in Fig. 2(f), the CIE coordinates of $Gd_2O_3:3\%\ Er^{3+}$ and $Gd_2O_3:3\%\ Er^{3+}, 10\%\ Na^+$ phosphors are calculated as $x=0.32$, $y=0.66$ and $x=0.35$, $y=0.64$, which fit well in the green areas.

The UCL mechanism of Er^{3+}, $Na^+/K^+/Cs^+$ co-doped Gd_2O_3 phosphors under 980 nm laser excitation was investigated. It is well known that the spectral intensity (I) of UC has a nonlinear relationship with the excitation power density (P). For the unsaturated UC process, the number of photons n required to transition from one level to another satisfies the following formula[35,36]:

$$I \propto P^n, \tag{1}$$

where I is the fluorescence intensity in any unit (arbitrary units), P is the excitation optical power (milliwatts), and n is the number of photons needed from the low-energy level to the high-energy level. Therefore, n is derived by the slope by linear fitting of curve of log I versus P. The power dependence of $Gd_2O_3:3\%\ Er^{3+}$ and $Gd_2O_3:3\%\ Er^{3+}, 10\%\ Na^+$ phosphors (at 563 and 661 nm) is shown in Figs. 3(a) and 3(b). Among them, the slope (n value) at 563 and 661 nm is 2.07 and 1.78 for $Gd_2O_3:3\%\ Er^{3+}$ phosphors, respectively, while the slope of phosphor decreased to 1.70 and 1.47 (563 and 661 nm) after the introduction of Na^+ ions, respectively. The power-dependent characteristics of $Gd_2O_3:3\%\ Er^{3+}, M^+$ (M = K, Cs) phosphors are shown in Figs. S4(a) and S4(d) (Supplementary Material). Compared with $Gd_2O_3:3\%\ Er^{3+}$, the n values at 563 and 661 nm are increased. These results indicate that although the luminescence can be significantly enhanced by doping, the green and red light emission of our sample is still explained by the two-photon process. The enhancement mechanism of Er^{3+}/Na^+ co-doped Gd_2O_3 was further investigated by the PL decay curves. As shown in Fig. 3(c), the emission lifetime is significantly prolonged after Na^+ doping, which is closely related to the crystallinity enhancement and surface reconstruction discussed above. The decay curves for the samples doped with K^+ or Cs^+ are shown in Figs. S4(b), S4(c) and S4(e), S4(f) (Supplementary Material), which also support the enhancement of UC emission caused by alkali metal ion doping. In addition, the UC emission mechanism related with the two-photon process is shown in Fig. 3(d). The Er^{3+} ion in the ground state is first excited to the $^4I_{11/2}$ level by absorbing a photon under the laser excitation at 980 nm, and then the Er^{3+} ions populated at the $^4I_{11/2}$ level continues to absorb a photon,

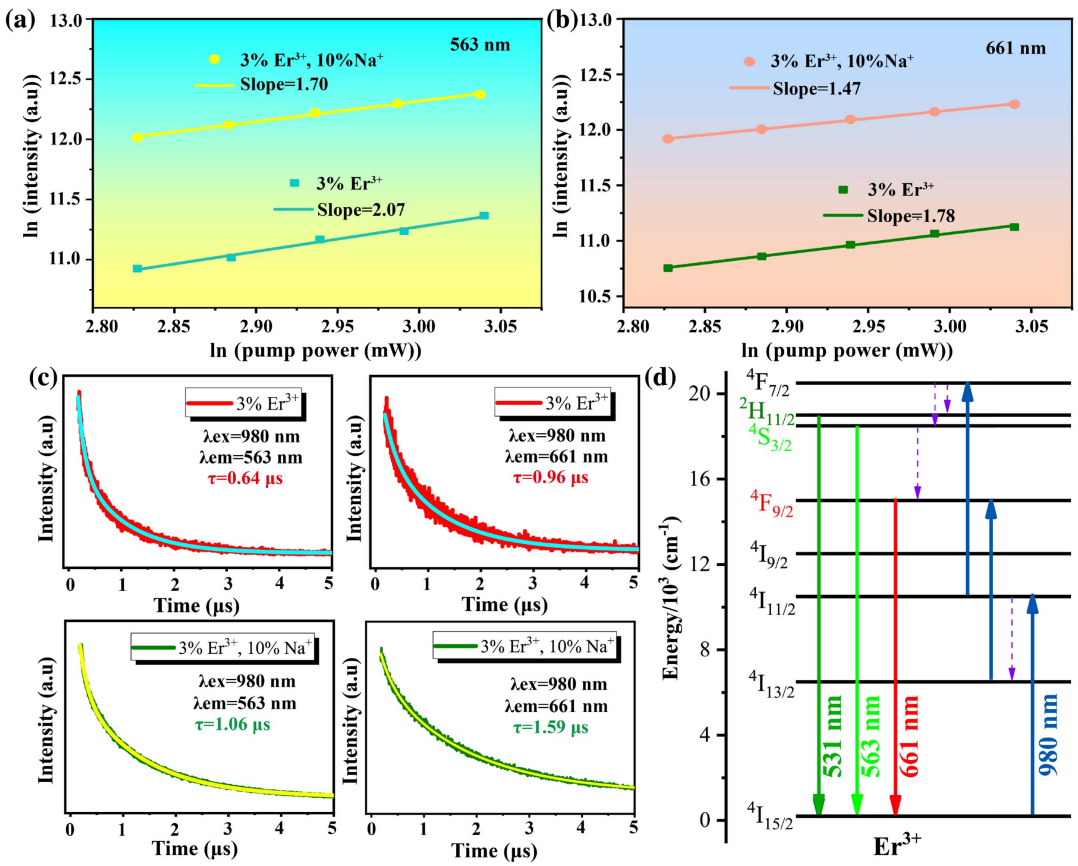

Fig. 3. (a), (b) Logarithmic patterns of power dependence of 3% Er^{3+} and 3% Er^{3+}, 10% Na^+-doped Gd_2O_3 sample materials in red and green wavebands; (c) emission attenuation curves of Gd_2O_3: 3% Er^{3+} and Gd_2O_3: 3% Er^{3+}, 10% Na^+ phosphors were fitted by a double exponential decay function (980 nm excitation); (d) possible UC mechanism of Er^{3+} ions under 980 nm excitation.

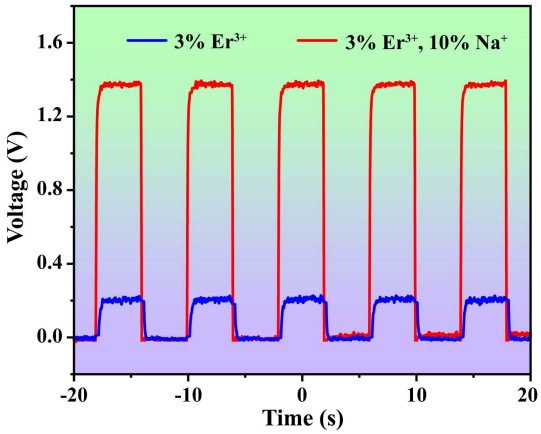

Fig. 4. Photocurrent response of the device incorporating Gd_2O_3: 3% Er^{3+}/PMMA and Gd_2O_3: 3% Er^{3+}, 10% Na^+/PMMA composite films under the square pulse with an NIR wavelength of 980 nm, the applied potential of 0 V, and 2 s off/on cycles.

leading to the population of the $^4F_{7/2}$ level. Afterwards, a nonradiative transition depopulates the $^4F_{7/2}$ level, resulting in the population of the $^2H_{11/2}$ and $^4S_{3/2}$ levels. Finally, the radiative transition of the $^2H_{11/2}$ and $^4S_{3/2}$ levels to the ground state produces visible green fluorescence. For red fluorescence associated with the transition of $^4F_{9/2}$ level to the ground state, there are two mechanisms. (1) Er^{3+} ions at the $^4S_{3/2}$ level can nonradiatively transition to the $^4F_{9/2}$ level through multiphonon relaxation. (2) After Er^{3+} is excited to the $^4I_{11/2}$ level, it is elevated to the $^4F_{9/2}$ level by a nonradiative relaxation process and the absorption of another photon. Obviously, the high green luminescence in Fig. 2(d) indicates that the former mechanism is more likely for the two-photon process in $Gd_2O_3:3\%\,Er^{3+}$, M^+ (M = Na, K, Cs) phosphors.

The UC phosphor particles were then integrated with a Si photoresistor for the demonstration of NIR photoresponse. In this device (see Section 2), the photocurrent response to the NIR light is related to the UC emission of the phosphor particles. In this work, the photocurrent responses of devices based on the $3\%\,Er^{3+}$ and $3\%\,Er^{3+}, 10\%\,Na^+$ doped phosphors that were excited by the concentrated NIR part of sunlight (by using a filter) were studied. In our experiment, a transparent gel formed by mixing phosphor powder and polymer is coated on the Si photoresistor to realize the conversion of the NIR light to an electrical response signal. Here, the excitation light is mechanically chopped to form a square-shaped signal with 2 s duration. The device shows no photovoltage response in a dark environment. Under optical excitation, the device based on the $Gd_2O_3:3\%\,Er^{3+}$/PMMA composite film only shows a weak photovoltage response of about 0.2 V, as shown in Fig. 4. In contrast, the photovoltage response of the device based on $Gd_2O_3:3\%\,Er^{3+}, 10\%\,Na^+$/PMMA composite film increased to 1.4 V. The results clearly suggest that $Gd_2O_3:3\%\,Er^{3+}$, $10\%\,Na^+$/PMMA composite film has a higher UC efficiency, so that the light response to the NIR part of the sunlight can be greatly enhanced. In addition, our device is stabler due to the encapsulation effect of the phosphor coated by a transparent polymer[37,38]. These results provide an effective strategy for the design and application of NIR light-responsive UC optoelectronic devices.

4. Conclusions

In summary, the crystal structure and surface properties of $Gd_2O_3:Er^{3+}$ and $Gd_2O_3:Er^{3+}, M^+$ (M = Na, K, Cs) phosphors have been systematically studied by a large number of microscopic methods. We are committed to discovering the universal features of enhanced UC efficiency after the introduction of alkali metal ions. The results show that the monocrystalline phase transition and surface optimization induced by the introduction of Na^+, K^+, and Cs^+ ions in $Gd_2O_3:Er^{3+}$ phosphors can significantly improve the UC intensity of phosphors. Meantime, the bar and column morphology may be more conducive to the UC PL process. In addition, an NIR-responsive device was demonstrated by coating a Si photoresistor with a transparent gel incorporating the UC powders. The photoelectric voltage is only 0.2 V for the device based on the $Gd_2O_3:3\%\,Er^{3+}$/PMMA film, while it goes up to 1.4 V for the device using $Gd_2O_3:3\%\,Er^{3+}, 10\%\,Na^+$/PMMA film. It is worth noting that, although Cs^+ ions doping has a higher UC intensity, it faces a large instability. In comparison, Na^+ ions have a higher performance due to their ubiquity and high UC efficiency.

Acknowledgement

This work was supported by the National Natural Science Foundation of China (No. 62105297), the Youth Backbone Teacher of Henan Province (No. 2020GGJS197), the Natural Science Foundation of Henan Province (212300410375), the Key Scientific Research Projects of Henan Province (No. 21A140018), the College Students Innovations Special Project (Nos. 202110482016, 202110482022, 202110482028, and 202210482004), the Excellent Team of Spectrum Technology and Application of Henan Province (No. 18024123007), the Open Research Fund Program of Henan Key Laboratory of Photoelectric Energy Storage Materials and Applications, Zhongyuan Yingcai Jihua (No. ZYYCYU202012144), the Quzhou Science and Technology Plan Projects (No. 18024123007), and the Key Laboratory of Advanced Micro-Structure Materials, Ministry of Education, Shanghai, China.

†These authors contributed equally to this work.

References

1. T. Han, Y. Wang, S. Ma, M. Li, N. Zhu, S. Tao, J. Xu, B. Sun, Y. Jia, Y. Zhang, S. Zhu, and B. Yang, "Near-infrared carbonized polymer dots for NIR-II bioimaging," Adv. Sci. **9**, 2203474 (2022).

2. M. Yang, J. Huang, J. Fan, J. Du, K. Pu, and X. Peng, "Chemiluminescence for bioimaging and therapeutics: recent advances and challenges," Chem. Soc. Rev. **49**, 6800 (2020).
3. H. Huang, S. Wang, R. Chen, N. Zhang, H.-R. Yao, Y. Zheng, F. Huang, and D. Chen, "Engineering upconverting core-shell nano-probe for spectral responsive fluid velocimetry," Nano Res. **16**, 1212 (2022).
4. M.-P. Zhuo, X.-D. Wang, and L.-S. Liao, "Recent progress of novel organic near-infrared-emitting materials," Small Sci. **2**, 2200029 (2022).
5. H. Altug, S. H. Oh, S. A. Maier, and J. Homola, "Advances and applications of nanophotonic biosensors," Nat. Nanotechnol. **17**, 5 (2022).
6. J. Li, L. Liu, X. Chen, C. Lu, H. Zhang, B. Li, C. Xue, and Z. Lou, "Dual-functional nonmetallic plasmonic hybrids with three-order enhanced upconversion emission and photothermal bio-therapy," Laser Photonics Rev. **16**, 2200197 (2022).
7. F. Zhang, S. Y. Park, C. Yao, H. Lu, S. P. Dunfield, C. Xiao, S. Uličná, X. Zhao, L. D. Hill, X. Chen, X. Wang, L. E. Mundt, K. H. Stone, L. T. Schelhas, G. Teeter, S. Parkin, E. L. Ratcliff, Y.-L. Loo, J. J. Berry, M. C. Beard, Y. Yan, B. W. Larson, and K. Zhu, "Metastable Dion-Jacobson 2D structure enables efficient and stable perovskite solar cells," Science **375**, 71 (2022).
8. L. Yang, J. Luo, L. Gao, B. Song, and J. Tang, "Inorganic lanthanide compounds with f-d transition: from materials to electroluminescence devices," J. Phys. Chem. Lett. **13**, 4365 (2022).
9. X. Feng, L. Lin, R. Duan, J. Qiu, and S. Zhou, "Transition metal ion activated near-infrared luminescent materials," Prog. Mater. Sci. **129**, 100973 (2022).
10. A. Shalav, B. S. Richards, T. Trupke, K. W. Krämer, and H. U. Güdel, "Application of $NaYF_4$:Er^{3+} up-converting phosphors for enhanced near-infrared silicon solar cell response," Appl. Phys. Lett. **86**, 013505 (2005).
11. W. Chen, A. G. Joly, and J. Z. Zhang, "Up-conversion luminescence of Mn^{2+} in ZnS:Mn^{2+} nanoparticles," Phys. Rev. B **64**, 041202 (2001).
12. F. Vetrone, R. Naccache, V. Mahalingam, C. G. Morgan, and J. A. Capobianco, "The active-core/active-shell approach: a strategy to enhance the upconversion luminescence in lanthanide-doped nanoparticles," Adv. Funct. Mater. **19**, 2924 (2009).
13. Q. Liu, H. Liu, D. Li, W. Qiao, G. Chen, and H. Ågren, "Microlens array enhanced upconversion luminescence at low excitation irradiance," Nanoscale **11**, 14070 (2019).
14. Y. Ji, W. Xu, N. Ding, H. Yang, H. Song, Q. Liu, H. Agren, J. Widengren, and H. Liu, "Huge upconversion luminescence enhancement by a cascade optical field modulation strategy facilitating selective multispectral narrow-band near-infrared photodetection," Light Sci. Appl. **9**, 2047 (2020).
15. W. Shao, G. Chen, A. N. Kuzmin, H. L. Kutscher, A. Pliss, T. Y. Ohulchanskyy, and P. N. Prasad, "Tunable narrow band emissions from dye-sensitized core/shell/shell nanocrystals in the second near-infrared biological window," J. Am. Chem. Soc. **138**, 16192 (2016).
16. H. Dong, L. D. Sun, and C. H. Yan, "Basic understanding of the lanthanide related upconversion emissions," Nanoscale **5**, 5703 (2013).
17. C. Mao, K. Min, K. Bae, S. Cho, T. Xu, H. Jeon, and W. Park, "Enhanced upconversion luminescence by two-dimensional photonic crystal structure," ACS Photonics **6**, 1882 (2019).
18. J. Xu, Z. Dong, M. Asbahi, Y. Wu, H. Wang, L. Liang, R. J. H. Ng, H. Liu, R. A. L. Vallee, J. K. W. Yang, and X. Liu, "Multiphoton upconversion enhanced by deep subwavelength near-field confinement," Nano Lett. **21**, 3044 (2021).
19. A. Das, C. Mao, S. Cho, K. Kim, and W. Park, "Over 1000-fold enhancement of upconversion luminescence using water-dispersible metal-insulator-metal nanostructures," Nat. Commun. **9**, 4828 (2018).
20. J. Li, W. Zhang, C. Lu, Z. Lou, and B. Li, "Nonmetallic plasmon induced 500-fold enhancement in the upconversion emission of the UCNPs/WO_{3-x} hybrid," Nanoscale Horiz. **4**, 999 (2019).
21. L. Jiang, X. Luo, Z. Luo, D. Zhou, B. Liu, J. Huang, J. Zhang, X. Zhang, P. Xu, and G. Li, "Interface and bulk controlled perovskite nanocrystal growth for high brightness light-emitting diodes," Chin. Opt. Lett. **19**, 030001 (2021).
22. Z. Zhang, W. Li, N. Ma, and X. Huang, "High-brightness red-emitting double-perovskite phosphor Sr_2LaTaO_6: Eu^{3+} with high color purity and thermal stability," Chin. Opt. Lett. **19**, 030003 (2021).
23. D. Zhou, D. Liu, W. Xu, Z. Yin, X. Chen, P. Zhou, S. Cui, Z. Chen, and H. Song, "Observation of considerable upconversion enhancement induced by $Cu_{2-x}S$ plasmon nanoparticles," ACS Nano **10**, 5169 (2016).
24. W. Zheng, B. Sun, Y. Li, T. Lei, R. Wang, and J. Wu, "Warm white broadband emission and tunable long lifetimes in Yb^{3+} doped Gd_2O_3 nanoparticles," Ceram. Int. **46**, 22900 (2020).
25. W. Zheng, B. Sun, Y. Li, R. Wang, T. Lei, and Y. Xu, "Near-infrared laser-triggered full-color tuning photon upconversion and intense white emission in single Gd_2O_3 microparticle," ACS Sustain. Chem. Eng. **8**, 2557 (2020).
26. W. Zheng, B. Sun, Y. Li, T. Lei, R. Wang, and J. Wu, "Low power high purity red upconversion emission and multiple temperature sensing behaviors in Yb^{3+}, Er^{3+} codoped Gd_2O_3 porous nanorods," ACS Sustain. Chem. Eng. **8**, 9578 (2020).
27. R. Priya, O. P. Pandey, and S. J. Dhoble, "Review on the synthesis, structural and photo-physical properties of Gd_2O_3 phosphors for various luminescent applications," Opt. Laser Technol. **135**, 106663 (2021).
28. N. Wei, X. Li, J. He, Y. Fan, Y. Dan, and J. Wang, "Design of an optical slot waveguide amplifier based on Er^{3+}-doped tellurite glass," Chin. Opt. Lett. **21**, 011404 (2023).
29. I. Kaminska, A. Wosztyl, P. Kowalik, B. Sikora, T. Wojciechowski, K. Sobczak, R. Minikayev, K. Zajdel, M. Chojnacki, W. Zaleszczyk, K. Lysiak, W. Paszkowicz, J. Szczytko, M. Frontczak-Baniewicz, W. Stryczniewicz, and K. Fronc, "Synthesis and characterization of Gd_2O_3:Er^{3+}, Yb^{3+} doped with Mg^{2+}, Li^+ ions-effect on the photoluminescence and biological applications," Nanotechnology **32**, 245705 (2021).
30. H. Liu, X. He, H. Jia, Y. Zheng, R. Bai, and Y. Zhang, "Investigation on the efficient up-conversion luminescence and temperature sensing properties of the Li^+/Er^{3+}/Yb^{3+}:Gd_2O_3 phosphor," Optik **228**, 166155 (2021).
31. A. Meza-Rocha, E. Huerta, E. Zaleta-Alejandre, Z. Rivera-Álvarez, and C. Falcony, "Enhanced photoluminescence of Y_2O_3:Er^{3+} thin films by Li^+ co-doping," J. Lumin. **141**, 173 (2013).
32. G. Chen, H. Liu, H. Liang, G. Somesfalean, and Z. Zhang, "Upconversion emission enhancement in Yb^{3+}/Er^{3+}-codoped Y_2O_3 nanocrystals by tridoping with Li^+ ions," J. Phys. Chem. C **112**, 12030 (2008).
33. G. Bi, L. Wang, W. Xiong, K. Ueno, H. Misawa, and J. Qiu, "Photoluminescence enhancement induced from silver nanoparticles in Tb^{3+}-doped glass ceramics," Chin. Opt. Lett. **10**, 092401 (2012).
34. B. Qian, H. Zou, D. Meng, X. Zhou, Y. Song, K. Zheng, C. Miao, and Y. Sheng, "Columnar Gd_2O_3:Eu^{3+}/Tb^{3+} phosphors: preparation, luminescence properties and growth mechanism," CrystEngComm **20**, 7322 (2018).
35. K. Saidi, M. Dammak, K. Soler-Carracedo, and I. R. Martin, "A novel optical thermometry strategy based on emission of Tm^{3+}/Yb^{3+} codoped $Na_3GdV_2O_8$ phosphors," Dalton Trans. **51**, 5108 (2022).
36. J. Xing, F. Shang, and G. Chen, "Upconversion luminescence of Yb^{3+}/Er^{3+} co-doped $NaSrPO_4$ glass ceramic for optical thermometry," Ceram. Int. **47**, 8330 (2021).
37. H. Jia, H. Jiang, Z. Chen, Z. Feng, X. Zhang, Y. Zhang, X. Xu, X. Li, F. Peng, X. Liu, and J. Qiu, "Near-infrared light-induced photoresponse in Er^{3+}/Li^+-codoped Y_2O_3/poly(methyl methacrylate) composite film," J. Phys. Chem. Lett. **13**, 3470 (2022).
38. P. Miluski, M. Kochanowicz, J. Zmojda, and D. Dorosz, "Luminescent properties of Tb^{3+}-doped poly(methyl methacrylate) fiber," Chin. Opt. Lett. **15**, 070602 (2017).